Journal of CO_2 Utilization 25 (2018) 254–263

Contents lists available at ScienceDirect

Journal of CO_2 Utilization

journal homepage: www.elsevier.com/locate/jcou

Contribution of thin films of ZrO_2 on TiO_2 nanotubes electrodes applied in the photoelectrocatalytic CO_2 conversion

João A. Lima Perini*, Juliano C. Cardoso, Juliana F. de Brito, Maria V. Boldrin Zanoni

São Paulo State University (UNESP), Institute of Chemistry, Rua Francisco Degni 55, 14800-060, Araraquara, SP, Brazil

ARTICLE INFO

Keywords:
CO_2 reduction
Adsorption
Photoelectrocatalysis
Zirconia
Methanol

ABSTRACT

Zirconium dioxide (ZrO_2) nanoparticles deposited on TiO_2 nanotube (NT) surfaces (30 nm of diameter) improved the photoelectrocatalytic conversion of carbon dioxide to fuel alcohol. The deposition of ZrO_2 nanoparticles was performed by a wet chemical deposition method, which provided excellent interaction with the nanotubular catalyst, as confirmed by surface analysis techniques. Methanol (485 μmol L^{-1}) and ethanol (268 μmol L^{-1}) were the main products generated under optimized condition after 60 min of the photoelectrochemical reduction of dissolved CO_2 in 0.1 mol L^{-1} Na_2SO_4 solution (pH 4.0) by Ti/TiO_2NT-ZrO_2 at −0.3 V *vs.* Ag/AgCl (3.0 mol L^{-1} KCl), under irradiation from an Hg lamp (120 mW cm^{-2}). The ZrO_2 deposits on Ti/TiO_2NT electrode surface amplified the photocurrent around 282% in −0.7 V, compared to Ti/TiO_2NT, increasing methanol and ethanol formation by 1054 and 2934%, respectively, after 60 min of the photoelectrocatalysis process. These results demonstrated the potential of using composites of Ti/TiO_2NT-ZrO_2 in photoelectrocatalytic reduction of dissolved CO_2 and contribute to the development of efficient technologies for fuel production and the reduction of pollutants emissions to the environment.

1. Introduction

The disturbance of the carbon dioxide cycle due to uncontrolled anthropogenic activity is well documented [1]. Although CO_2 is vital for life on Earth, in recent decades there have been substantial increases in atmospheric CO_2, decreased absorption of carbon dioxide by vegetation, and increased diffusion of the gas into the oceans (affecting the pH), all of which contribute to climate change. As a result, there are intensified efforts to identify ways to decrease emissions, as well as to remove and sequestrate CO_2, and to use it to produce valuable products [2].

Among various methods described for the conversion of CO_2, increasing attention has been focused on photocatalytic processes that can convert CO_2 to marketable products such as methanol, ethanol, formic acid, methane, and others, under irradiation in the presence of a catalyst at low temperature and pressure [3–5]. The method consists of the photoirradiation of a semiconductor surface that acts as a catalyst, with the creation of charge carriers (electron/hole pairs, e^-/h^+) by photons with energy higher than the band gap energy. The electrons on the catalyst surface promote the reduction of CO_2 to hydrocarbons. Although the process has been successful in several studies [3–5], the recombination of the charge carriers decreases their availability at the catalyst surface, hence decreasing the efficiency in the process. An additional difficulty is the lack of selectivity of the process.

The photoelectrocatalysis technique can provide superior performance, compared to photocatalysis, and has been recently been shown to be highly successful for the reduction of CO_2 [6–11]. The multiple-step process of CO_2 reduction by photoelectrocatalysis is complex and is limited (i) by the strength of CO_2 adsorption on the substrate surface, (ii) by the transfer of multiple photogenerated electrons (the conversion to methanol requires 6 electrons), and (iii) by the formation of protons for the production of a hydrocarbon from the carbon dioxide [12].

Another important variable in CO_2 reduction by photoelectrocatalysis is the semiconductor employed in the reaction. The literature reports the use of different p-type semiconductors (GaP, GaAs, CdS, and InP) to photoelectrochemically reduce CO_2 [13–17]. TiO_2 is a very useful semiconductor due to its stability, cost-effectiveness, nontoxicity, and ability to participate in a variety of photoelectrocatalytic processes, including oxidation of organic compounds [18,19], inactivation of microorganisms [20], and water splitting [3]. However, it is inefficient in the direct reduction of CO_2, because CO_2 adsorption is not favored [21] and the electrons photoexcited to the conduction band of TiO_2 (E_{cb} ~ −0.25 V) are not compatible with the energy required for the CO_2/CH_3OH reduction (E° ~ −0.4 V *vs.* NHE).

The use of p-n type semiconductor heterojunctions has been explored as a way to enhance the photoelectrocatalytic performance of

* Corresponding author.
E-mail address: joao.perini@unesp.br (J.A.L. Perini).

https://doi.org/10.1016/j.jcou.2018.04.005
Received 19 January 2018; Accepted 6 April 2018
Available online 22 April 2018

photoelectrodes [10,22–26]. The heterojunction can improve the separation of electron/hole pairs, since the charge transfer can be amplified. Most studies of p-n type semiconductors concern arrangements of copper and/or copper oxides with TiO_2 as an effective way to increase the photoreduction of CO_2. However, information is lacking concerning the potential use of two n-n semiconductors with different band gaps, such as TiO_2-ZrO_2 electrodes, for the photoelectroreduction of CO_2.

Although, ZrO_2 is known to be a poor photocatalyst, due its wide band gap (5.0 eV), which requires photoexcitation at $\lambda < 250$ nm [27], the literature reports that the energy level diagram of ZrO_2 can change due to oxygen point defects and the energy level can reaches values around 3.4 eV [28]. In addition, ZrO_2 can provide effective sites for the adsorption of CO_2 [29,30] that is very important in photoelectrocatalytic process. The variety of catalytically active sites in the Zr^{4+} O_2^- pairs [29], mainly associated with Lewis acid sites favors the adsorption of CO_2. The literature reports [31,32] that ZrO_2 presented good photocatalytic activity under irradiation at wavelengths < 250 nm, for the splitting of water and the reduction of carbonate in solution. Besides that, Kohno et al. [33–35] also reported that ZrO_2 could reduce CO_2 by photolysis in the presence of H_2, forming $HCOO^-$ and CO. Therefore, the decoration of TiO_2 nanotubes by ZrO_2 could improve the electrode characteristics and the selective reduction of CO_2.

The present work investigates, for the first time, the use of ZrO_2 as a modifier of Ti/TiO_2NT electrodes and its applicability in the photoelectrocatalytic reduction of CO_2. The Ti/TiO_2NT electrodes were prepared by electrochemical oxidation in a fluoride medium and were decorated with ZrO_2 by wet chemical deposition. The CO_2 reduction to methanol and ethanol was dramatically increased at Ti/TiO_2NT-ZrO_2 even when irradiated by commercial Hg lamp (120 mW cm^{-2}) and under bias potential of −0.3 V. The CO_2 conversion has been evaluated through chromatographic techniques and parameters such as electrolyte, potential and pressure were investigated to assess the effectiveness of the purposed method.

2. Experimental

2.1. Ti/TiO_2NT preparation and decoration with ZrO_2

Ti/TiO_2NT electrodes were prepared by electrochemical anodization of titanium sheets (Realum, São Paulo, Brazil), using NH_4F (0.25% m/v) as the electrolyte in glycerol:water (90:10 v/v) medium. A potential of 30 V was applied during 50 h, using a DC power supply (MPL-1303, Minipa, São Paulo, Brazil), in a two-electrode cell with a DSA (dimensionally stable anodes, Ru/Ir/TiO_2) (De Nora, São Paulo, Brazil) counter electrode. The electrodes were subsequently annealed for 2 h at 450 °C in a muffle furnace (Model 3 P-S, EDG, São Paulo, Brazil), as described previously [36].

Ti/TiO_2NT-ZrO_2 electrodes were prepared by a wet chemical deposition method, adapted from Li et al. [37]. The Ti/TiO_2NT electrodes were immersed in a solution of 0.02 M $ZrCl_4$ (Sigma-Aldrich, St. Louis, MO, USA) and the pH was adjusted to pH 10 with NH_4OH, forming precipitated $Zr(OH)_4$. After 2 h of reaction, the electrodes were washed with Milli-Q water, dried for 1 h at 105 °C in an oven (Model SL-100, Solab, São Paulo, Brazil), and annealed for 2 h at 450 °C, resulting in the Ti/TiO_2NT-ZrO_2 semiconductor.

2.2. Characterization of the materials

The prepared Ti/TiO_2NT and Ti/TiO_2NT-ZrO_2 electrodes were characterized by X-ray diffraction (XRD) using a diffractometer (Model D500, Siemens, Munich, Germany) operated with Cu Kα radiation. Morphological characterization was carried out by field emission gun scanning electron microscopy (FEG-SEM), using a Model 7500 F microscope (JEOL, Tokyo, Japan). High resolution transmission electron microscopy (TEM) images were acquired using a CM Super Twin 200 instrument (Philips/FEI, Eindhoven, The Netherlands) operated at 200 kV. The samples were prepared by ultrasonically dispersing the catalyst into isopropyl alcohol, and then placing a drop of this suspension onto a copper grid. X-ray photoemission spectra (XPS) were obtained using an ESCA + system (Scienta Omicron Nanotechnology, Taunusstein, Germany) equipped with an EA125 hemispherical analyzer and an XM 1000 monochromated Al Kα X-ray source (1486.7 eV). An Omicron CN10 charge neutralizer with beam energy of 1.6 eV was used for charge effects compensation. The XPS results were corrected using C1s calibration energy of 284.8 eV.

Electronic properties were evaluated using photocurrent curves recorded by cyclic voltammetry and linear sweep voltammetry, at scan rates of 100 mV s^{-1}, in the potential range from −0.7 to 1.5 V, with and without irradiation, using an Autolab PGSTAT 302 N potentiostat/galvanostat (Metrohm, Herisau, Switzerland). Optical properties were evaluated by diffuse reflectance spectroscopy, using a Cary 60 UV-vis spectrometer (Agilent Technologies, Santa Clara, CA, USA) equipped with an external diffuse reflectance accessory probe (Barrelino™, Harrick Scientific, Pleasantville, NY, USA). The equipment was calibrated with a Spectralon standard (Labsphere USRS-99-020, 99% reflectance) and the reflectance and absorbance were measured in the range 200–800 nm.

Fourier transform infrared (FTIR) spectra were recorded using a diamond attenuated total reflection accessory and a Vertex 70 spectrometer (Bruker, Ettlingen, Germany) equipped with a LADTGS detector, in the spectral range 4000–450 cm^{-1}.

2.3. CO_2 photoelectroreduction

Photoelectrocatalytic experiments were performed by applying a controlled current density or a controlled potential, using two-electrode and three-electrode systems, respectively, in a 250 mL cylindrical one-compartment stainless steel reactor (Fig. SI1A). Current was applied to the Ti/TiO_2NT-ZrO_2 working electrode irradiated with UV–vis light from a 125 W high pressure mercury lamp (Philips, The Netherlands), positioned 0.5 cm from the electrode. A DSA was used as the anode (auxiliary electrode). The radiation intensity of the lamp was measured in the UVA region (320–400 nm) using a radiometer (PMA 2100, Solar Light Co., Glenside, PA, USA), with the sensor placed at the same angle as the reactor. The photoreaction performed at controlled current density was carried out in 200 mL of aqueous supporting electrolyte containing CO_2 dissolved by bubbling CO_2 gas (Oxi-Ara, São Paulo, Brazil) for 20 min at 6 atm pressure. The experiments carried out at a controlled applied potential utilized the same reactor, with the addition of an Ag/AgCl (3.0 M KCl) reference electrode (Fig. SI1B). In this case, a pressure of 1 atm was used, with continuous bubbling of CO_2 throughout the experiment.

2.4. Quantification of products in photoelectrochemical CO_2 reduction

Methanol and ethanol were analyzed by gas chromatography with flame ionization detection (GC-FID) (Model 2010, Shimadzu, Kyoto, Japan), after solid phase microextraction (SPME) using an SPME fiber coated with divinylbenzene/polydimethylsiloxane (DVB/PDMS) (type 57329-U, Supelco, Saint Quentin Fallavier, France). A 0.5 mL aliquot of solution was transferred to a closed container (1.5 mL) and heated in a water bath (Model HB 0.5, IKA, São Paulo, Brazil) for 7 min. The fiber was exposed to the vapor for 5 min and was then inserted into the gas chromatograph. A 30 m Stabilwax column was used (0.25 mm internal diameter, 25 µm film thickness; Restek, Bellefonte, PA, USA). The carrier gas was nitrogen, at a flow rate of 1.0 mL min^{-1}, and the injector and detector temperatures were 250 °C. The heating ramp was from 40 °C to 46 °C, at 2 °C min^{-1}, followed by an increase to 170 °C at 45 °C min^{-1} and maintaining the final temperature for 3 min. Calibration curves for methanol and ethanol determination showed linearity in the range from 2 to 2500 µmol L^{-1}. The determination

coefficients were 0.99 for both alcohols and the detection limits were 1.11 and 0.81 μmol L^{-1} for methanol and ethanol, respectively.

The gas phase products (CO, CH_4, and H_2) were analyzed by gas chromatography with thermal conductivity detection (GC-TCD), using a Model 2014 instrument (Shimadzu, Kyoto, Japan) equipped with a Carboxen-1010 PLOT fused silica capillary column (30 m × 0.53 mm, 0.30 μm; Supelco, Bellefonte, PA, USA). The column heating program was from 130 to 135 °C, at 46 °C min^{-1}, a hold for 5 min, followed by an increase to 200 °C at 46 °C min^{-1}, and maintaining the final temperature for 2 min. The injector and detector temperatures were 220 and 230 °C, respectively. Argon was used as the carrier gas.

Oxygen concentrations were measured using an oximeter (Model 407510, Extech Instruments, Waltham, MA, USA).

Carboxylic acids were analyzed using a high performance liquid chromatography (HPLC) system (LC 20AT Prominence, Shimadzu, Kyoto, Japan) equipped with a diode array detector (DAD). Separation was achieved using a reversed phase Rezex ROA-Organic Acid H+ (8%) ion-exclusion column (300 × 7.8 mm, 8 μm; Phenomenex, Torrance, CA, USA). Isocratic elution (1 mL min^{-1}) was performed with a mobile phase of 2.5 mM H_2SO_4. The detection wavelength was 210 nm.

Full scan profiles of the reaction products were obtained using a gas chromatography-mass spectrometry (GC–MS) system (Agilent Technologies, Santa Clara, CA, USA) consisting of a Model 7980B chromatograph connected to a Model 5977 A mass selective detector and a Model 7693 autosampler. The separation was performed using an HP-5 fused silica capillary column (30 m × 0.25 mm × 0.25 μm; Agilent, USA). Helium was used as the carrier gas, at a flow rate of 1.0 mL min^{-1}. The injector temperature and heating ramp were the same as used for the GC-FID analysis. The mass spectrometric detector was operated in multiple reaction monitoring mode, with ionization energy of 70 eV, quadrupole temperature of 150 °C, and scanning from *m/z* 50 to 500.

The generation of hydroxyl radicals was estimated by the bleaching of N,*N*-dimethyl-4-nitrosoaniline (RNO) solution (97%, Sigma Aldrich, St Louis, MO, USA), using a Cary 60 UV–vis spectrophotometer (Agilent Technologies, Santa Clara, CA, USA) [38,39]. RNO acts as a probe compound in a pseudo-first order reaction with hydroxyl radicals, which decreases the intensity of the characteristic RNO band at 440 nm, according to Eq. (1):

$$\ln \frac{[RNO]}{[RNO]_0} = k_{obs} t \quad (1)$$

where $k_{obs} = k \times [HO]ss$, $k = 1.25 \times 10^{10}\ M^{-1}\ s^{-1}$ [39], $[RNO]_0$ = initial concentration of RNO, [RNO] = concentration of RNO at time t, and [HO]ss = steady state concentration of HO.

The steady state rate of HO production can be obtained from the slope of the semi-log plot (Fig. SI2).

3. Results and discussion

3.1. Characterization of the Ti/TiO_2NT and Ti/TiO_2NT-ZrO_2 electrodes

The FEG-SEM images (Fig. 1A) revealed the formation of self-aligned and self-organized nanotubes grown perpendicularly on the titanium sheet substrates by electrochemical anodization and annealing at 450 °C. The well distributed nanotubes presented average wall thickness and diameter of 30 and 106 nm, respectively. After deposition of the ZrO_2 nanoparticles, the average wall thickness increased to 33 nm. There were also nanoparticle agglomerates with average diameter of 76 nm on the Ti/TiO_2NT surface after application of the wet chemical deposition method during 2 h (Fig. 1B). It could be concluded that the deposition preferentially occurred around the nanotubes and that deposition of ZrO_2 over longer periods led to greater agglomeration. Such agglomeration was therefore avoided decreasing the time deposits of ZrO_2 (2 h) since it decreased the photoactivity. The presence of ZrO_2 on the TiO_2 was confirmed using high resolution TEM. The micrograph obtained for the Ti/TiO_2NT-ZrO_2 sample (Fig. 1C) showed the presence of a TiO_2 nanotube with distance of 3.51 Å relative to the (101) plane of the anatase phase, which was the same phase observed at highest intensity in the X-ray diffractogram of Ti/TiO_2NT (Fig. 1D). The presence of ZrO_2 was also observed from the lattice spacing of the (−111) plane, measured as 3.16 Å, and was confirmed by the X-ray diffractogram of the Ti/TiO_2NT-ZrO_2 (Fig. 1D). A TEM image of the TiO_2 nanotubes with nanoparticles on the surfaces of the tubes is shown in Fig. SI3.

The presence of the ZrO_2 nanoparticles on the TiO_2 nanotubes was also revealed by the X-ray diffractograms of the Ti/TiO_2NT before and after modification with the ZrO_2 nanoparticles (Fig. 1D). Analysis of the diffractogram using the CrystMet database showed the presence of diffraction peaks related to the anatase phase of TiO_2 at 2θ of 25.5°, 48.2°, 54.2°, 55.2°, and 70.5°, which is indexed to the (101), (200), (105), (211), and (220) planes, respectively (ID458591). Two small peaks of the rutile phase of TiO_2 were also observed at 2θ of 35.8° and 75.9°, related to the (101) and (202) planes, respectively (ID461090). The presence of ZrO_2 was confirmed by the new peak observed in the diffractogram after ZrO_2 deposition, at 2θ of 28°, related to the (−111) plane of a monoclinic zirconia nanophase (ID182372), in agreement with the morphology shown in the TEM image (Fig. 1C). Although the anatase phase may be more photoactive than the rutile phase [40–42], the latter presents a different absorption wavelength (≤420 nm for rutile and ≤400 nm for anatase) [41]. Consequently, the small amount of rutile phase, relative to the anatase phase, can increase the light absorption spectrum of the TiO_2 semiconductor, hence improving the photoactivity of the material [42].

The XPS spectrum of Ti/TiO_2NT-ZrO_2 (Fig. 2A) showed the presence of Zr 3d, C 1s, Ti 2p, and O 1s transitions. The XPS analysis showed the presence of ZrO_2 in the semiconductor, with a double peak at 181.3 and 183.6 eV (Fig. 2B) reflecting the Zr $3d_{5/2}$ and Zr $3d_{3/2}$ transitions of ZrO_2 [43], confirming the successful modification of the TiO_2 nanotubes with ZrO_2.

3.2. Photoactivity of Ti/TiO_2NT-ZrO_2 electrodes

Fig. 3A shown the photocurrent *vs.* potential curves obtained for Ti/TiO_2NT and Ti/TiO_2NT-ZrO_2 electrodes and both were compared under dark and UV–vis irradiation in 0.1 mol L^{-1} Na_2SO_4 before and after dissolution of CO_2. The Ti/TiO_2NT electrode (Curve 1) showed no photocurrent under dark conditions. On the other hand, under UV-vis irradiation, e^-/h^+ pairs are generated at the electrode surface and a well-defined photocurrent appeared above −0.20 V (Curve 2). As reported previously, under these conditions water oxidation and hydroxyl radical formation can occur at the electrode surface [44].

Ti/TiO_2NT-ZrO_2 also showed no current under dark conditions (data not shown). However, under UV–vis light there was a higher photocurrent (Curve 3), with an improvement of 87% at 1.0 V, compared to the unmodified Ti/TiO_2NT (Fig. SI4). This could be explained by the fact that the ZrO_2 nanoparticles acted as efficient electron traps, minimizing e^-/h^+ recombination and indicating a lower band gap energy associated with the ZrO_2 deposited on the TiO_2 surface. In the cathodic region (Curve 3), there was a shift in the current to less negative potential, compared to the irradiated Ti/TiO_2NT indicating that ZrO_2 also improves the hydrogen generation. In the presence of CO_2 in the same experimental conditions, the I_{ph} *vs.* E curves showed a decreasing of the photocurrent in the cathodic region of 208% and 187% for Ti/TiO_2NT (Curve 4) and Ti/TiO_2NT-ZrO_2 (Curve 5), respectively. This behavior suggested that the CO_2 in solution can be acting as a scavenger of photogenerated electrons [24,45], consequently reducing the photocurrent.

The optical properties of Ti/TiO_2NT, Ti/TiO_2NT-ZrO_2, and ZrO_2 powder were investigated by the acquisition of UV–vis absorption spectra (Fig. 3B). The spectrum for the ZrO_2 powder exhibited transparency in the visible region (Curve 3), while Ti/TiO_2NT-ZrO_2 (Curve

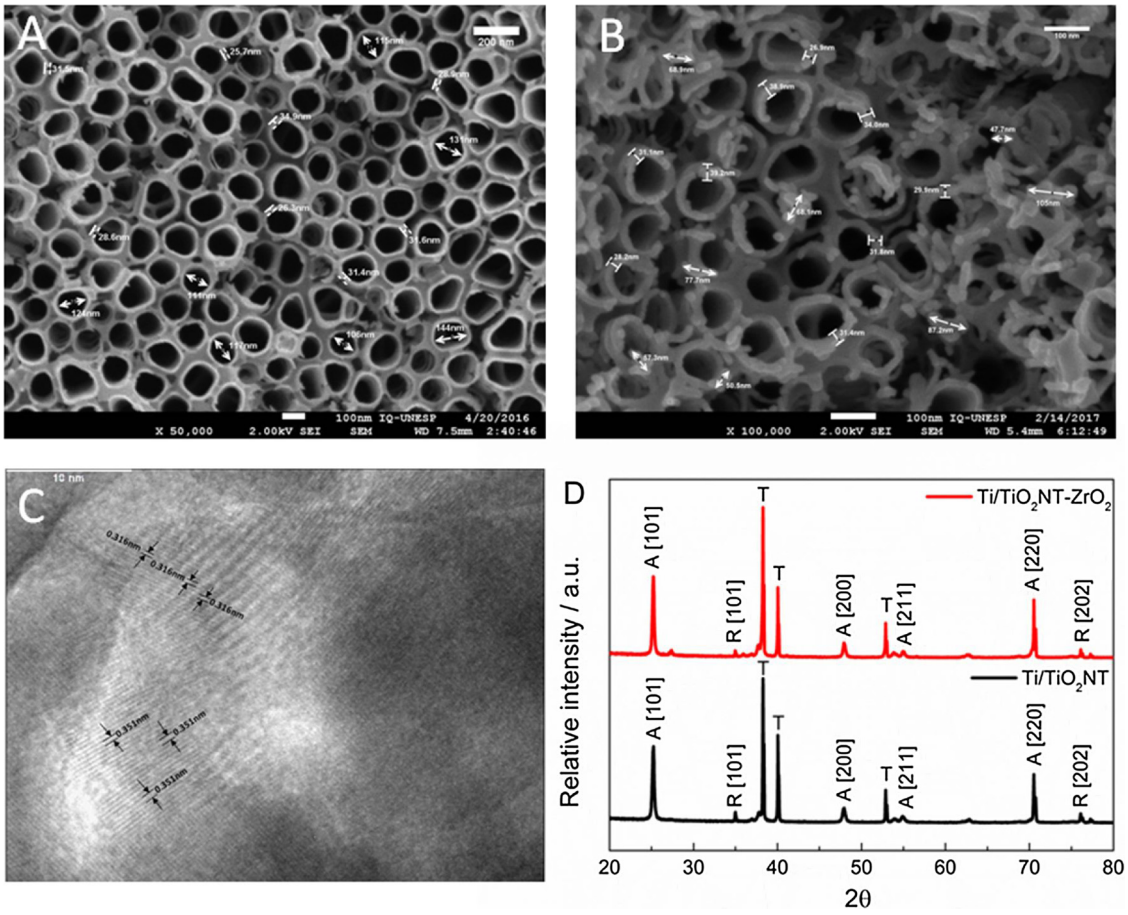

Fig. 1. FEG-SEM images of (A) Ti/TiO_2NT and (B) Ti/TiO_2NT-ZrO_2. (C) TEM images of Ti/TiO_2NT-ZrO_2. (D) X-ray diffractograms of Ti/TiO_2NT and Ti/TiO_2NT-ZrO_2.

2) showed a slight increase in the absorption in the visible region, compared to the bare Ti/TiO_2NT electrode (Curve 1). This behavior indicated that the addition of ZrO_2 at the TiO_2 surface could slightly alter the band gap of the material, as calculated from the Tauc plot [46] using Eq. (2), where α is the absorption coefficient, *h* is Planck's constant (J s), υ is the frequency (s^{-1}), and γ is the power coefficient. This method consists of extrapolating the linear portion of a plot of $\alpha(h\upsilon)^{1/\gamma}$ as a function of hυ (eV), and the intercept at α = 0 is the optical band gap (Eg, in eV). The diffuse reflectance measurements (data not shown) could be converted to an equivalent absorption coefficient using the Kubelka-Munk method (Eq. (3)). The band gap values obtained were 3.0 eV for Ti/TiO_2NT-ZrO_2 and 3.2 eV for the bare Ti/TiO_2NT, as shown in the insert of Fig. 3B. ZrO_2 semiconductors typically have a band gap of 5.0 eV [31], although it has been reported that the value can vary and reach 3.0 eV, depending on the size of the material [47].

$$\alpha(h\upsilon)\alpha(h\upsilon - Eg)^{\gamma} \quad (2)$$

$$\text{K-M} \approx \alpha = \frac{(1 - R)^2}{2R} \quad (3)$$

However, although the change in band gap was not so marked, further studies were carried out to understand how is the adsorption of CO_2 at Ti/TiO_2NT-ZrO_2 using photoeletrocatalytic reduction at controlled current density and controlled potential.

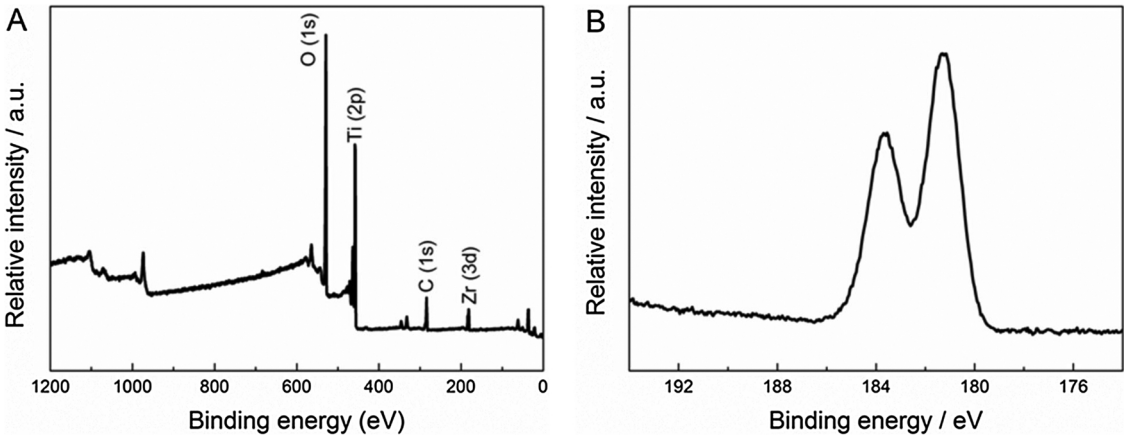

Fig. 2. (A) Survey scan XPS spectra in the binding energy range 0–1200 eV of Ti/TiO_2NT-ZrO_2. (B) High resolution Zr 3d spectra.

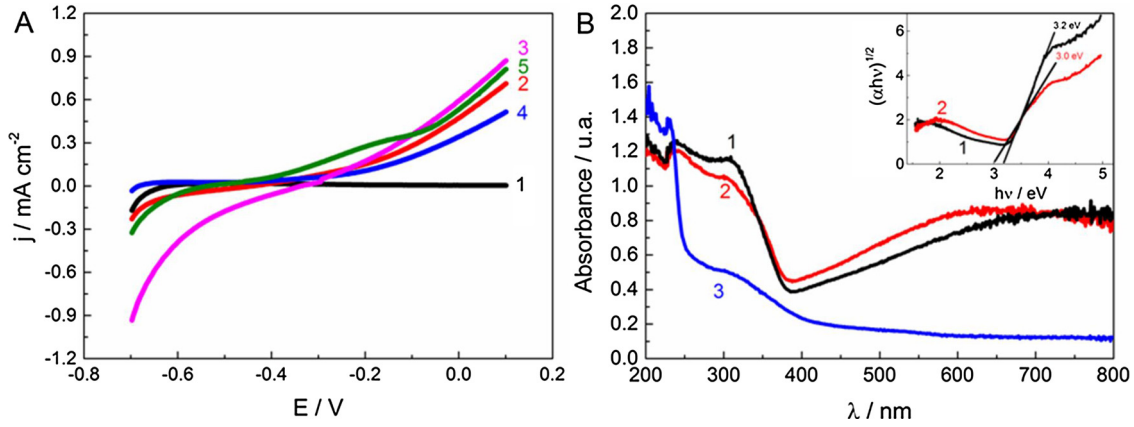

Fig. 3. (A) Linear sweep voltammograms obtained for the Ti/TiO_2NT electrode in the dark (1), irradiated by UV–vis light without CO_2 (2) and saturated with CO_2 (4), and for the Ti/TiO_2NT-ZrO_2 electrode under UV–vis light without CO_2 (3) and saturated with CO_2 (5). (B) UV–vis absorption spectra of Ti/TiO_2NT (1), Ti/TiO_2NT-ZrO_2 (2), and ZrO_2 powder (3), with inset of Tauc plots showing the band gaps of Ti/TiO_2NT (1) and Ti/TiO_2NT-ZrO_2 (2). Experimental conditions: 0.1 mol L^{-1} Na_2SO_4; scan rate = 10 mV s^{-1}.

3.3. Photoelectrochemical CO_2 reduction under UV-vis irradiation and controlled current density

Firstly, the performances of the Ti/TiO_2NT and Ti/TiO_2NT-ZrO_2 electrodes were investigated in the reduction of CO_2 during 60 min of photoelectrocatalysis in 0.1 mol L^{-1} Na_2SO_4 saturated with CO_2, at pH 4.0, under UV–vis irradiation (125 W; 120 mW cm^{-2}). Photoelectrolysis was performed at a controlled current density of −1.0 mA cm^{-2} and pressure of 6.0 atm, in order to simplify the photoelectrocatalytic reactor and increase the solubility of CO_2 in the aqueous solution. Fig. 4A illustrates the results obtained for alcohol formation after photoelectroreduction of CO_2 at the Ti/TiO_2NT and Ti/TiO_2NT-ZrO_2 electrodes. The formation of methanol and ethanol was higher at the Ti/TiO_2NT-ZrO_2 electrode (544 and 109 μmol L^{-1}, respectively), compared to the undecorated bare TiO_2 electrode (142 and 17 μmol L^{-1}, respectively. The much higher formation of CO_2 reduction products at the Ti/TiO_2NT-ZrO_2 electrode was due to the ability of ZrO_2 to adsorb CO_2 molecules on the surface, as reported elsewhere [29,30,48].

In order to understand the effect of pressure on the

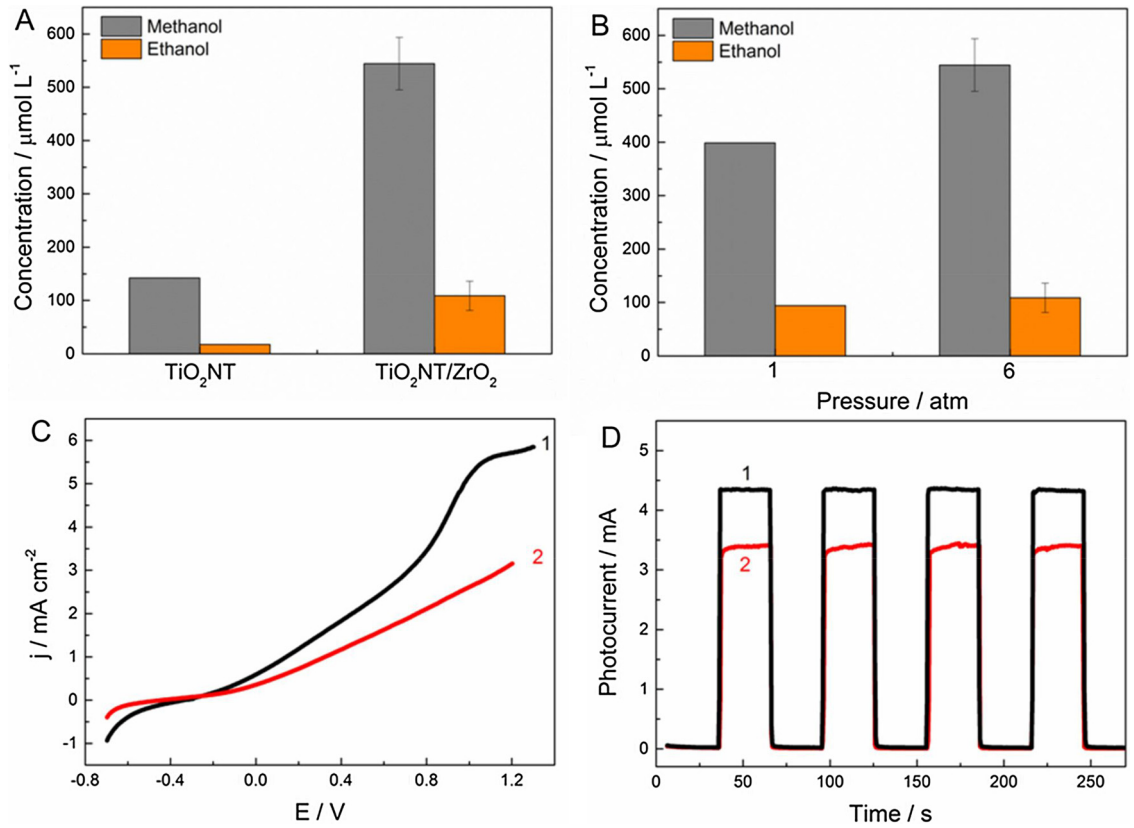

Fig. 4. (A) Evaluation of products formed by photoelectrocatalytic CO_2 reduction in 0.1 mol L^{-1} Na_2SO_4, at 6 atm pressure and an applied current density of −1 mA cm^{-2}, using Ti/TiO_2NT and Ti/TiO_2NT-ZrO_2. (B) Evaluation of products formed by photoelectrocatalytic CO_2 reduction in 0.1 mol L^{-1} Na_2SO_4, at 1 and 6 atm pressure and an applied current density of −1 mA cm^{-2}, using Ti/TiO_2NT-ZrO_2. (C) Linear sweep voltammograms and (D) photocurrents for Ti/TiO_2NT-ZrO_2 in 0.1 mol L^{-1} Na_2SO_4, before (1) and after (2) applying a current density of −1 mA cm^{-2}.

photoelectrocatalytic CO_2 reduction, experiments were performed at different pressures (Fig. 4B). A pressure of 1 atm resulted in generation of 399 and 94 μmol L^{-1} of methanol and ethanol, respectively. When the pressure applied to the photoelectrocatalytic system was increased, the generation of methanol and ethanol increased by 37% and 16%, respectively, probably due to greater solubility of CO_2 at higher pressure. Furthermore, it has been found that methanol can act as an intermediate in the photoelectrocatalytic formation of ethanol [6,8], so an increase in the methanol concentration could lead to an increase in ethanol generation, due to the subsequent conversion reaction.

The CO_2 concentration in the electrolyte and mass transport are important determinations of the faradaic efficiency of product formation. Therefore, an increase of the system pressure increased the CO_2 solubility (33 mM at 25 °C and 1 atm CO_2) and consequently improved the faradaic efficiency for reduction of CO_2 [49]. Kaneco et al. [50] studied the photocatalytic reduction of CO_2 over TiO_2 powder using high pressure. The generation of methane, the main reaction product, increased with increasing pressure, reaching concentrations of 0.1–1.2 μmol L^{-1} when pressures between 2 and 28 atm were applied. In other work, methanol generation increased rapidly up to 10 atm of pressure, followed by a rapid decline as the pressure was increased further [51]. In the present case, however, high pressure was not essential for improving product generation, indicating that the use of Ti/TiO_2NT-ZrO_2 for adsorption of CO_2 was more effective than pressure. Therefore, the subsequent experiments were performed at the usual pressure of 1 atm.

Promising results were obtained for the generation of CO_2 reduction products at the Ti/TiO_2NT-ZrO_2 electrode when a current density of −1.0 mA cm^{-2} was applied. However, the electrode was only stable for a short photoelectrocatalysis time. The voltammetric curves and photocurrent responses obtained before and after application of a current density of −1.0 mA cm^{-2} are shown in Fig. 4C and D, respectively. Both curves showed a substantial decrease in the photoactivity after photoelectrolysis at the Ti/TiO_2NT-ZrO_2 electrode. At a controlled current density, the cell potential was around −2.5 V, resulting in an excessive amount of hydrogen gas formed on the photoelectrode surface. These bubbles led to release of the ZrO_2 nanoparticles from the electrode surface and subsequent major expansion in the TiO_2 lattice. According to Zhou and Zhang [52], H^+ intercalation and H_2 evolution eventually leads to the cleavage of Ti—O bonds, forming oxygen vacancies, or even the destruction of TiO_2 nanotubes at applied potentials below −1.8 V, as was the case for the potential reached in the present work. Furthermore, at potentials smaller than −0.942 V, ZrO_2 is reduced to metallic zirconium [53], leading to the release of zirconium from the Ti/TiO_2NT surface. Therefore, subsequent photoelectrolysis experiments were performed at controlled potential.

3.4. Photoelectrochemical CO_2 reduction at controlled potential under UV-vis irradiation

Fig. 5A shows the effect of applied potential in the range from −1.0 to 0.0 V *vs.* Ag/AgCl on the photoelectroreduction of CO_2. The experiments were conducted during 60 min of photoelectrocatalysis in 0.1 mol L^{-1} Na_2SO_4 saturated with CO_2, at pH 4.0, under UV–vis irradiation at ambient pressure. The generation of formic acid, acetic acid, formaldehyde, acetaldehyde, acetone, propanol, carbon monoxide, and hydrogen was monitored by HPLC-DAD, GC-FID, GC-TCD, and GC–MS, as described in the Experimental section. However, under the optimized conditions, only methanol and ethanol were satisfactorily quantified (Fig. SI5), and no other products were present in measurable amounts. The high selectivity for methanol and ethanol formation during photoelectrocatalytic CO_2 reduction has been reported previously [24,54–56]. Generation of methanol and ethanol occurred at all the different potentials, but the highest generation of alcohol was achieved at −0.3 V, reaching values of 485 μmol L^{-1} for methanol and 268 μmol L^{-1} for ethanol. The mechanism by which the catalytic CO_2 photoreaction occurs on semiconductors remains controversial and strongly depends on the materials, the reaction conditions, irradiation, electrolyte, pH, and other parameters [45]. The CO_2 molecule is inert and stable, so its reduction by an electron to generate the anion radical ($CO_2^{\cdot -}$) requires a high electrochemical potential of approximately −1.9 V *vs.* NHE. In the present case, with photoelectrocatalysis using the Ti/TiO_2NT-ZrO_2 electrode, the direct reduction of CO_2 to a stable $CO_2^{\cdot -}$ intermediate occurred at a low bias potential of around −0.3 V *vs.* Ag/AgCl. Analyses of H_2 in the tests at potentials of −0.7 and −0.3 V showed no evidence of its production during the photoelectrocatalytic CO_2 reduction process, indicating the high selectivity of the Ti/TiO_2NT-ZrO_2 electrode for the generation of methanol and ethanol.

In order to explain the influence of the applied potential, cyclic voltammograms were recorded using Ti/TiO_2NT-ZrO_2 in 0.1 mol L^{-1} Na_2SO_4 at pH 4.0 in the dark. The results are shown in Fig. 5B. The reduction peak indicated that at −0.6 V, Zr(IV) was reduced to Zr(II) oxides. The results corroborated previous work by Peng et al. [53] indicating that at lower potential, ZrO_2 was probably reduced to zirconium oxide (the lowest oxidation state) [53], which does not seem to have the same activity in the adsorption of CO_2 as ZrO_2. Furthermore, when more negative potentials (−1.0 and −0.7 V) were applied, self-doping in the TiO_2 lattice by the Ti^{3+} intermediate [44] could have resulted in lower generation of methanol and ethanol, which did not occur at a more positive potential (−0.3 V).

Fig. 6A compares the performances of the Ti/TiO_2NT and Ti/TiO_2NT-ZrO_2 electrodes in the photoelectrochemical reduction of CO_2 to methanol and ethanol. The photoreduction of CO_2 to methanol and ethanol was very low at Ti/TiO_2NT, achieving only 42 μmol L^{-1} of methanol and 8.8 μmol L^{-1} of ethanol, while yields at Ti/TiO_2NT-ZrO_2 were 485 and 268 μmol L^{-1}, respectively. In the case of the TiO_2 nanotubes, the adsorption of CO_2 at the Ti/TiO_2NT surface was slow (Fig. 6B; Curve 1) and the Fermi energy level and the formal potential of CO_2/CH_3OH were not sufficiently aligned to allow electron transfer to CO_2 [44]. On the other hand, zirconium oxide appeared to provide excellent sites for CO_2 adsorption (Curve 3), and similar bands in the range 2365–2358 cm^{-1} have been observed previously for adsorption of CO_2 at the ZrO_2 surface [48]. In interactions with various metal oxides, CO_2 associates with a surface Lewis acid center *via* σ-coordination from one of the oxygen lone pairs [29]. The coordination of the CO_2 molecule with the surface of ZrO_2 occurs linearly, as described by Bensitel et al. [48]. Therefore, during photoelectrocatalysis, irradiation of the catalyst surface ($h\upsilon > $ band gap) generates e^-/h^+ pairs, so that the excited electron in the conduction band moves to the surface, resulting in reduced adsorption of CO_2 on the ZrO_2 surface.

Although ZrO_2 presents a wide band gap of approximately 5.0 eV and a high negative flat band potential (E_{fb}) of −1.0 eV *vs.* NHE, at pH 0 [57], it appears that its deposition onto Ti/TiO_2 nanotubes, followed by annealing at 450 °C, results in an excellent material to improve CO_2 absorption. On the other hand, TiO_2 has a band gap of 3.0 eV and a flat band potential of 0.05 eV *vs.* NHE, at pH 0 [58]. Sayama and Arakawa [31] reported that the lowest conduction band potential was similar to the flat band potential, and the highest potentials in the valence bands of ZrO_2 and TiO_2 were estimated to be 4.0 and 2.95 eV, respectively (*vs.* NHE, at pH 0). This would prevent the transport of an electron from the TiO_2 conduction band to the ZrO_2 conduction band (Fig. 6A). However, Foster et al. [28], using plane wave density functional theory calculations, showed that monoclinic ZrO_2 could have defects on its structure, with oxygen interstitials (O_3° and O_3^{-}) and vacancies (V_4^{2+} and V_4^{+}) acting as electron traps, and V_4° vacancies acting as hole traps. These defects could cause the ZrO_2 band gap to decrease by up to 2.07 eV. Considering the behavior of the Ti/TiO_2NT-ZrO_2 material, the TiO_2 and ZrO_2 conduction bands were closer than expected, enabling the transfer of electrons between the oxides. Further transfer of electrons from ZrO_2 to adsorbed CO_2 readily formed $CO_2^{\cdot -}$ as an intermediate for alcohol formation.

The effect of the supporting electrolyte was investigated using

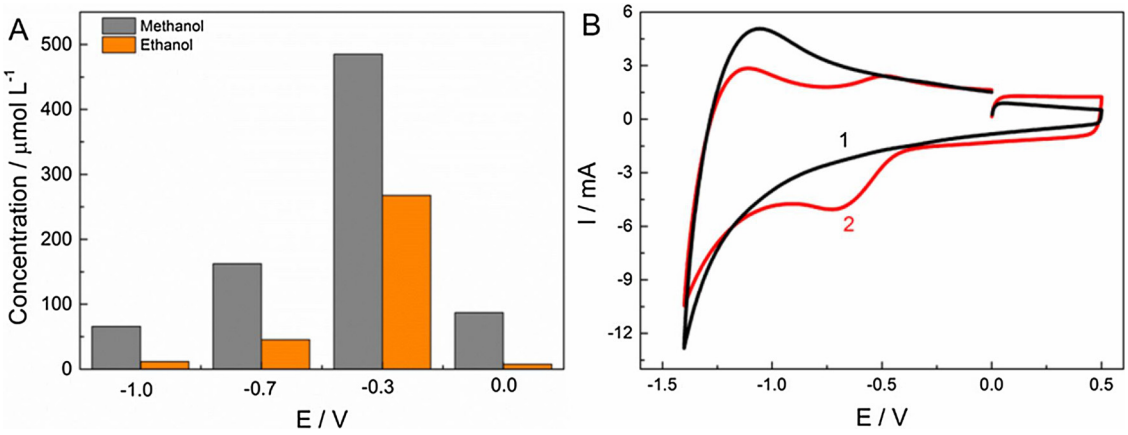

Fig. 5. (A) Effect of potential on products formed by photoelectrocatalytic CO_2 reduction in 0.1 mol L^{-1} Na_2SO_4 at 1 atm pressure, using Ti/TiO_2NT-ZrO_2. (B) Cyclic voltammetry curves obtained for the Ti/TiO_2NT (1) and Ti/TiO_2NT-ZrO_2 (2) electrodes in 0.1 mol L^{-1} Na_2SO_4, in the range from −1.4 to 0.5 V, with a scanning speed of 100 mV s^{-1}.

solutions of sodium sulfate, sodium bicarbonate, and sodium chloride, with the Ti/TiO_2NT-ZrO_2 electrode at a bias potential of −0.3 V and UV–vis irradiation during 60 min, at 1 atm pressure. In the work of Brito et al. [6], greatest methanol formation was achieved using 0.1 mol L^{-1} of supporting electrolyte, so this concentration was used in all the experiments. After bubbling CO_2 for 30 min, the Na_2SO_4 and NaCl electrolyte solutions presented pH values of 4.0, while the Na_2CO_3 solution showed a pH of 8.2.

The results indicated that the CO_2 photoelectroreduction resulted in higher methanol (485 μmol L^{-1}) and ethanol (268 μmol L^{-1}) formation in sodium sulfate electrolyte, compared to the NaCl and Na_2CO_3 solutions, where methanol generation did not exceed 100 μmol L^{-1} and ethanol generation was negligible (Fig. 7A). The better performance of CO_2 reduction in the Na_2SO_4 electrolyte could be explained by the different diffusion coefficients of Na_2SO_4, NaCl, and Na_2CO_3. The CO_2 diffusion coefficient is 1.91×10^{-9} m^2 s^{-1}, while Cl^- and CO_3^{2-} have diffusion coefficients of the same order of magnitude (2.03×10^{-9} and 0.92×10^{-9} m^2 s^{-1}, respectively) [59]. In contrast, the diffusion coefficient of SO_4^{2-} is around 3.00×10^{-12} m^2 s^{-1} [60], 1000 times smaller than the others, which probably facilitated the mobility of CO_2 in the solution.

Ghadimkhani et al. [7] used Na_2SO_4 as supporting electrolyte for photoelectroreduction of CO_2 using a hybrid CuO/Cu_2O electrode and found that this medium was selective for methanol formation. In other work, much higher formation of methanol was obtained using Na_2SO_4 electrolyte (pH 6), achieving approximately 800 μmol L^{-1}, compared to the use of Na_2CO_3 (pH 8), employing electrodes of copper(II) aspirinate complex deposited onto nanotubes of TiO_2, with application of −0.35 V [24]. However, Brito et al. [45] showed that when a potential of −0.6 V was applied, the best electrolyte was $NaHCO_3$ (pH 8), while when a potential of 0.2 V was used, there was greater product formation when K_2SO_4 was used (pH 8). These results showed that in addition to optimization of the semiconductor material used for the catalysis, the operational conditions (electrolyte and applied bias potential) also have to be optimized in order to maximize the generation of CO_2 reduction products. In the present case, of the best performance of the Ti/TiO_2NT-ZrO_2 electrode was obtained in sulfate electrolyte, which was therefore employed in the subsequent measurements.

Using the optimized conditons, the influence of reaction time on the CO_2 photoelectroreduction was investigated in experiments carried out for 120 min using a bias potential of −0.3 V in sodium sulfate solution at Ti/TiO_2NT-ZrO_2 electrode irradiated with UV–vis light, at 1 atm pressure. The generation of methanol and ethanol reached 219 and 144 μmol L^{-1}, respectively, after 30 min of photoelectrolysis (Fig. 7B). After a longer reaction time (60 min), the concentrations of the CO_2 reduction products increased to 524 μmol L^{-1} of methanol and 265 μmol L^{-1} of ethanol. However, after 120 min of photoelectrocatalysis, the concentrations of the alcohols (216 μmol L^{-1} of methanol and 40 μmol L^{-1} of ethanol) were lower than obtained after the first 30 min.

The decreases in the alcohol concentrations were probably due to further oxidation by hydroxyl radicals (HO, −2.73 V *vs.* NHE) formed at the counter electrode. The positively charged DSA counter electrode could generate HO by the oxidation of water [8,61], resulting in

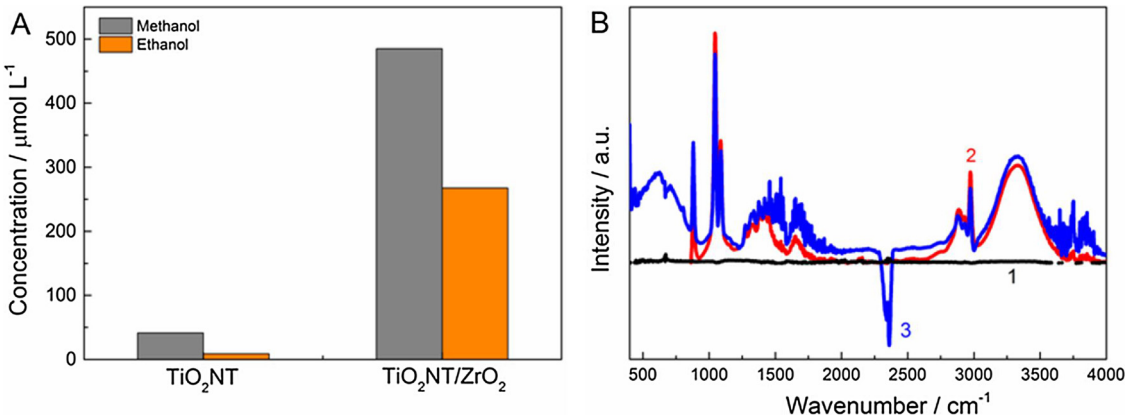

Fig. 6. (A) Evaluation of products formed by photoelectrocatalytic CO_2 reduction in 0.1 mol L^{-1} Na_2SO_4, at 1 atm pressure and applying −0.3 V, using Ti/TiO_2NT and Ti/TiO_2NT-ZrO_2. (B) Infrared spectra of Ti/TiO_2NT (1) and Ti/TiO_2NT-ZrO_2 in the absence (2) and presence (3) of CO_2.

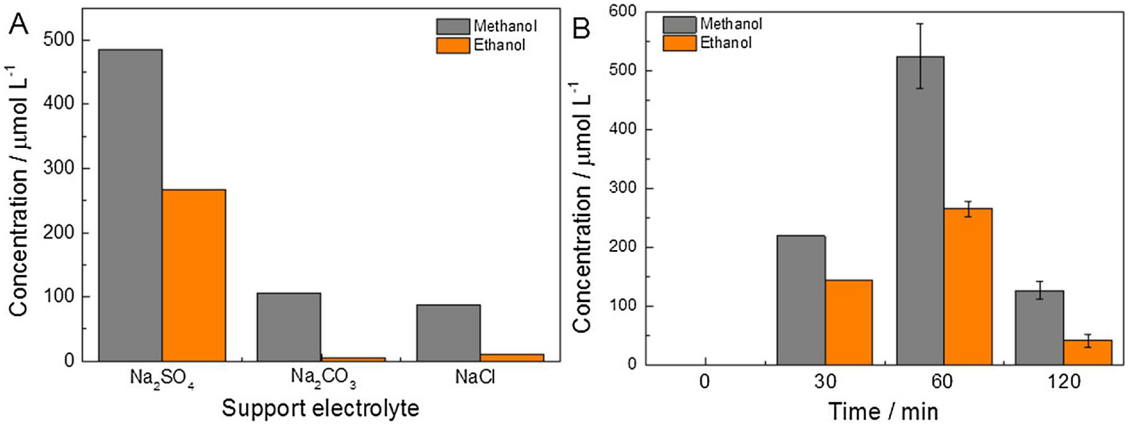

Fig. 7. (A) Effect of supporting electrolyte (at 0.1 mol L^{-1}) on products formation for photoelectrocatalytic CO_2 reduction using Ti/TiO_2NT-ZrO_2 at 1 atm pressure and applying −0.3 V. (B) Evaluation of products formed during photoelectrocatalytic CO_2 reduction using Ti/TiO_2NT-ZrO_2 in 0.1 mol L^{-1} Na_2SO_4, at 1 atm pressure and applying −0.3 V.

oxidation of the products formed during the photoreduction of CO_2, after longer electrolysis times. In the present case, the steady state concentration of HO during the photoelectroreduction of CO_2 was 6.6×10^{-18} mol L^{-1}. Therefore, successive oxidation of methanol and ethanol could potentially form aldehydes, ketones, carboxylic acids, or even CO_2, which were not identified in the experiments. In addition, oxygen could be formed as a water oxidation product at the counter electrode, in reactions involving the hydroxyl radical [61]. However, O_2 was not found in the present work. Therefore, further experiments required a photoelectrocatalysis time of 60 min in order to maximize the generation of alcohols.

3.5. Effects of photoelectrocatalysis, photocatalysis, and electrocatalysis on CO_2 reduction

The efficiencies of photocatalysis, electrocatalysis, and photoelectrocatalysis in the reduction of CO_2 were compared, considering the effects of UV–vis irradiation and the applied potential individually and in combination. The electrochemical reduction was performed using Ti/TiO_2NT-ZrO_2, applying a potential of −0.3 V in sodium sulfate electrolyte (0.1 mol L^{-1}) at pH 4.0 (with bubbling CO_2 for 30 min) and ambient pressure. The photochemical reduction of CO_2 was performed using the Ti/TiO_2NT-ZrO_2 electrode irradiated with UV–vis light, in 0.1 mol L^{-1} Na_2SO_4, at pH 4.0 and 1 atm pressure. The photoelectrochemical reduction was carried out with application of a potential of −0.3 V and UV–vis irradiation, in 0.1 mol L^{-1} Na_2SO_4, at pH 4.0 and 1 atm pressure.

The electrocatalysis technique using Ti/TiO_2NT-ZrO_2 resulted in negligible generation of methanol (9.2 µmol L^{-1}) and ethanol (4.7 µmol L^{-1}) during 60 min of reaction, while the photocatalysis produced larger amounts of the alcohols (47 and 194 µmol L^{-1}, respectively) (Fig. 8). Sayama and Arakawa [31] evaluated the photocatalytic reduction of CO_2 using ZrO_2 powder under a 400 W high pressure Hg lamp and obtained only 2.5 µmol L^{-1} h^{-1} of carbon monoxide, with no formation of methanol, formic acid, or methane. Despite the high band gap energy of ZrO_2, the adsorbed carbonate derived from CO_2 can be photoexcited on the surface of ZrO_2 and converted to $CO_2^{\cdot -}$, which reacts with hydrogen to form organic molecules such as methanol and ethanol [62]. In addition, irradiation of Ti/TiO_2NT with photon energy higher than the band gap (3.2 eV) can cause an excited electron to reach the conduction band of TiO_2 and then be promoted to the conduction band of the ZrO_2, hence amplifying the reduction of CO_2 to $CO_2^{\cdot -}$.

Photoelectrocatalysis carried out at the Ti/TiO_2NT-ZrO_2 electrode with application of −0.3 V, under UV–vis irradiation, resulted in the production of 485 µmol L^{-1} of methanol (Fig. 8). The amount of methanol generated increased by 5171% and 932%, relative to electrocatalysis and photocatalysis, respectively. Furthermore, the sum of the electrocatalytic and photocatalytic processes generated much less methanol and ethanol, compared to the photoelectrocatalytic process, demonstrating the importance of the bias potential.

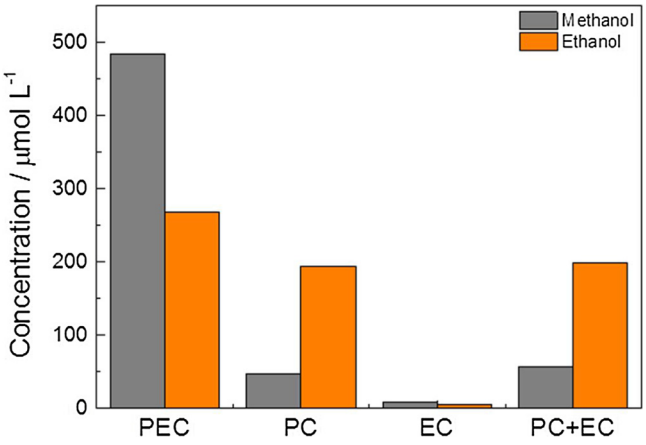

Fig. 8. Evaluation of products formed by catalytic CO_2 reduction using photoelectrocatalysis (PEC), photocatalysis (PC), and electrocatalysis (EC) with Ti/TiO_2NT-ZrO_2 at 1 atm pressure in 0.1 mol L^{-1} Na_2SO_4. E_{app} = −0.3 V.

4. Conclusions

This study demonstrated that the addition of ZrO_2 as a thin film on a Ti/TiO_2 nanotubes electrode resulted in excellent photoelectrochemical performance in the reduction of CO_2. Photoelectrocatalysis in 0.1 mol L^{-1} sodium sulfate solution saturated with CO_2, at pH 4.0 and 1 atm pressure, under UV-vis irradiation and with an applied potential of only −0.3 V, resulted in generation of high amounts of methanol (485 µmol L^{-1}) and ethanol (268 µmol L^{-1}). The findings indicated that although ZrO_2 may be considered a poor photocatalyst, due its high band gap and high negative flat band, the variety of catalytically active sites and the presence of Lewis acid sites favored the adsorption of CO_2. Therefore, ZrO_2 can be considered a valuable material for use in the reduction of CO_2, deserving further investigation for the development of new photoelectrocatalytic systems for CO_2 reduction.

Acknowledgements

The authors are grateful to FAPESP (#2014/50945-1 and #2015/18109-4) and INCT-DATREN (#465571/2014-0) for support of this

work. J.A.L.P. and J.F.B. received scholarships from FAPESP (#2016/18057-7 and #2013/25343-8). J.C.C. received a scholarship from CNPq (#152274/2016-2).

Appendix A. Supplementary data

Supplementary material related to this article can be found, in the online version, at doi:https://doi.org/10.1016/j.jcou.2018.04.005.

References

[1] G.A. Olah, A. Goeppert, G.K.S. Prakash, Chemical recycling of carbon dioxide to methanol and dimethyl ether: from greenhouse gas to renewable, environmentally carbon neutral fuels and synthetic hydrocarbons, J. Org. Chem. 74 (2008) 487–498, http://dx.doi.org/10.1021/jo801260f.

[2] G. Centi, S. Perathoner, Opportunities and prospects in the chemical recycling of carbon dioxide to fuels, Catal. Today 148 (2009) 191–205, http://dx.doi.org/10.1016/j.cattod.2009.07.075.

[3] T. Inoue, A. Fujishima, S. Konishi, K. Honda, Photoelectrocatalytic reduction of carbon dioxide in aqueous suspensions of semiconductor powders, Nature 277 (1979) 637–638, http://dx.doi.org/10.1038/277637a0.

[4] S. Neatu, J.A. Maciá-Agulló, H. Garcia, Solar light photocatalytic CO_2 reduction: general considerations and selected bench-mark photocatalysts, Int. J. Mol. Sci. 15 (2014) 5246–5262, http://dx.doi.org/10.3390/ijms15045246.

[5] S. Xie, Q. Zhang, G. Liu, Y. Wang, Photocatalytic and photoelectrocatalytic reduction of CO_2 using heterogeneous catalysts with controlled nanostructures, Chem. Commun. 52 (2015) 35–59, http://dx.doi.org/10.1039/C5CC07613G.

[6] J.F. Brito, A.R. Araújo, K. Rajeshwar, M.V.B. Zanoni, Photoelectrochemical reduction of CO_2 on Cu/Cu_2O films: product distribution and pH effects, Chem. Eng. J. 264 (2015) 302–309, http://dx.doi.org/10.1016/j.cej.2014.11.081.

[7] G. Ghadimkhani, N.R. de Tacconi, W. Chanmanee, C. Janaky, K. Rajeshwar, Efficient solar photoelectrosynthesis of methanol from carbon dioxide using hybrid CuO-Cu_2O semiconductor nanorod arrays, Chem. Commun. 49 (2013) 1297, http://dx.doi.org/10.1039/c2cc38068d.

[8] T.T. Guaraldo, J.F. Brito, D. Wood, M.V.B. Zanoni, A New Si/TiO_2/Pt p-n junction semiconductor to demonstrate photoelectrochemical CO_2 conversion, Electrochim. Acta 185 (2015) 117–124, http://dx.doi.org/10.1016/j.electacta.2015.10.077.

[9] P. Li, J. Xu, H. Jing, C. Wu, H. Peng, J. Lu, H. Yin, Wedged N-doped CuO with more negative conductive band and lower overpotential for high efficiency photoelectric converting CO_2 to methanol, Appl. Catal. B Environ. 156–157 (2014) 134–140, http://dx.doi.org/10.1016/j.apcatb.2014.03.011.

[10] G.K. Mor, O.K. Varghese, R.H.T. Wilke, S. Sharma, K. Shankar, T.J. Latempa, K. Choi, C.A. Grimes, p-Type Cu-Ti-O nanotube arrays and their use in self-biased heterojunction photoelectrochemical diodes for hydrogen generation, Nano Lett. 8 (2008) 1906–1911.

[11] K. Rajeshwar, N.R. De Tacconi, G. Ghadimkhani, W. Chanmanee, C. Janáky, Tailoring copper oxide semiconductor nanorod arrays for photoelectrochemical reduction of carbon dioxide to methanol, ChemPhysChem 14 (2013) 2251–2259, http://dx.doi.org/10.1002/cphc.201300080.

[12] K. Bhattacharyya, A. Danon, B. Vijayan, K. Gray, P. Stair, E. Weitz, Role of the surface Lewis acid and base sites in the adsorption of CO_2 on titania nanotubes and platinized titania nanotubes: an in situ FT-IR study, J. Phys. Chem. C 117 (2013) 12661–12678.

[13] B. Aurian-Blajani, M. Halmann, J. Manassem, Electrochemical measurements on the photo- electrochemical reduction of aqueous carbon dioxide on p-gallium phosphide and p-gallium arsenide semiconductor electrodes, Sol. Energy Mater. 8 (1983) 425–440.

[14] H. Fujiwara, H. Hosokawa, K. Murakoshi, Y. Wada, S. Yanagida, Surface characteristics of ZnS nanocrystallites relating to their photocatalysis for CO2 reduction, Langmuir 14 (1998) 5154–5159, http://dx.doi.org/10.1021/la9801561.

[15] T. Arai, S. Sato, K. Uemura, T. Morikawa, T. Kajino, T. Motohiro, Photoelectrochemical reduction of CO_2 in water under visible-light irradiation by a p-type InP photocathode modified with an electropolymerized ruthenium complex, Chem. Commun. 46 (2010) 6944–6946, http://dx.doi.org/10.1039/c0cc02061c.

[16] H. Kim, H. Kim, J. Kim, W. Kim, W. Choi, Enhanced photocatalytic and photoelectrochemical activity in the ternary hybrid of CdS/TiO_2/WO_3 through the cascadal electron transfer, J. Phys. Chem. C 115 (2011) 9797–9805, http://dx.doi.org/10.1021/jp1122823.

[17] Y. Lin, R. Kapadia, J. Yang, M. Zheng, K. Chen, M. Hettick, X. Yin, C. Battaglia, I.D. Sharp, J.W. Ager, A. Javey, Role of TiO_2 surface passivation on improving the performance of p-InP photocathodes, J. Phys. Chem. C 119 (2015) 2308–2313, http://dx.doi.org/10.1021/jp5107313.

[18] J.C. Cardoso, T.M. Lizier, M.V.B. Zanoni, Highly ordered TiO_2 nanotube arrays and photoelectrocatalytic oxidation of aromatic amine, Appl. Catal. B Environ. 99 (2010) 96–102, http://dx.doi.org/10.1016/j.apcatb.2010.06.005.

[19] G.G. Bessegato, J.C. Cardoso, M.V.B. Zanoni, Enhanced photoelectrocatalytic degradation of an acid dye with boron-doped TiO_2 nanotube anodes, Catal. Today 240 (2015) 100–106, http://dx.doi.org/10.1016/j.cattod.2014.03.073.

[20] M.F. Brugnera, M. Miyata, G.J. Zocolo, C.Q.F. Leite, M.V.B. Zanoni, Ti/TiO_2 nanotubes enhance mycobacterium fortuitum, mycobacterium chelonae and mycobacterium abscessus inactivation in water, J. Chem. Technol. Biotechnol. 89 (2013) 1686–1696, http://dx.doi.org/10.1002/jctb.4243.

[21] K. Kocí, L. Obalova, L. Matejová, D. Plachá, Z. Lacný, J. Jirkovský, O. Solcová, Effect of TiO_2 particle size on the photocatalytic reduction of CO_2, Appl. Catal. B Environ. 89 (2009) 494–502, http://dx.doi.org/10.1016/j.apcatb.2009.01.010.

[22] S. Sato, T. Arai, T. Morikawa, K. Uemura, T.M. Suzuki, H. Tanaka, T. Kajino, Selective CO_2 conversion to formate conjugated with H_2O oxidation utilizing semiconductor/complex hybrid photocatalysts, J. Am. Chem. Soc. 133 (2011) 15240–15243, http://dx.doi.org/10.1021/ja204881d.

[23] M.R. Hasan, S.B. Abd Hamid, W.J. Basirun, S.H. Meriam Suhaimy, A.N. Che Mat, A sol–gel derived, copper-doped, titanium dioxide–reduced graphene oxide nanocomposite electrode for the photoelectrocatalytic reduction of CO_2 to methanol and formic acid, RSC Adv. 5 (2015) 77803–77813, http://dx.doi.org/10.1039/c5ra12525a.

[24] S. Stülp, J.C. Cardoso, J.F. de Brito, J.B.S. Flor, R.C.G. Frem, F.A. Sayão, M.V.B. Zanoni, An artificial photosynthesis system based on Ti/TiO_2 coated with Cu (II) aspirinate complex for CO_2 reduction to methanol, Electrocatalysis 8 (2017) 279–287, http://dx.doi.org/10.1007/s12678-017-0367-9.

[25] J. Qu, X. Zhang, Y. Wang, C. Xie, Electrochemical reduction of CO_2 on RuO_2/TiO_2 nanotubes composite modified Pt electrode, Electrochim. Acta 50 (2005) 3576–3580, http://dx.doi.org/10.1016/j.electacta.2004.11.061.

[26] T. Yui, A. Kan, C. Saitoh, K. Koike, T. Ibusuki, O. Ishitani, Photochemical reduction of CO_2 using TiO_2: effects of organic adsorbates on TiO_2 and deposition of Pd onto TiO_2, ACS Appl. Mater. Interfaces 3 (2011) 2594–2600, http://dx.doi.org/10.1021/am200425y.

[27] C.C. Lo, C.H. Hung, C.S. Yuan, J.F. Wu, Photoreduction of carbon dioxide with H_2 and H_2O over TiO_2 and ZrO_2 in a circulated photocatalytic reactor, Sol. Energy Mater. Sol. Cells 91 (2007) 1765–1774, http://dx.doi.org/10.1016/j.solmat.2007.06.003.

[28] A.S. Foster, V.B. Sulimov, F. Lopez Gejo, A.L. Shluger, R.M. Nieminen, Modelling of point defects in monoclinic zirconia, J. Non Cryst. Solids 303 (2002) 101–107, http://dx.doi.org/10.1016/S0022-3093(02)00974-2.

[29] C. Morterra, L. Orio, Surface characterization of zirconium oxide II. The interaction with carbon dioxide at ambiebt temperature, Mater. Chem. Phys. 24 (1990) 247–268, http://dx.doi.org/10.1016/0254-0584(90)90089-S.

[30] B. Bachiller-Baeza, I. Rodriguez-Ramos, A. Guerrero-Ruiz, Interaction of carbon dioxide with the surface of zirconia, Langmuir 14 (1998) 3556–3564, http://dx.doi.org/10.1021/la970856q.

[31] K. Sayama, H. Arakawa, Photocatalytic decomposotion of water and photocatalytic reduction of carbon dioxide over ZrO_2 catalyst, J. Phys. Chem. 97 (1993) 22–24, http://dx.doi.org/10.1021/j100105a001.

[32] K. Sayama, H. Arakawa, Effect of carbonate addition on the photocatalytic decompostion of liquid water over a ZrO_2 catalyst, J. Photochem. Photobiol. A Chem. 94 (1996) 67–76, http://dx.doi.org/10.1039/a607662i.

[33] Y. Kohno, T. Tanaka, T. Funabiki, S. Yoshida, Photoreduction of carbon dioxide with hydrogen over ZrO_2, Chem. Commun. (1997) 841–842, http://dx.doi.org/10.1039/A700185A.

[34] Y. Kohno, H. Hayashi, S. Takenaka, T. Tsunehiro, T. Fanabiki, S. Yoshida, Photo-enhanced reduction of carbon dioxide with hydrogen over Rh/TiO_2, J. Photochem. Photobiol. A Chem. 126 (1999) 117–123, http://dx.doi.org/10.1016/S1010-6030(99)00113-6.

[35] Y. Kohno, T. Tanaka, T. Funabiki, S. Yoshida, Photoreduction of CO2 with H2 over ZrO2. A study on interaction of hydrogen with photoexcited CO2, Phys. Chem. Chem. Phys. 2 (2000) 2635–2639, http://dx.doi.org/10.1039/b001642j.

[36] J.C. Cardoso, M.V.B. Zanoni, Structural effects of nanotubes, nanowires, and nanoporous Ti/TiO_2 electrodes on photoelectrocatalytic oxidation of 4,4-oxydianiline, Sep. Sci. Technol. 45 (2010) 1628–1636, http://dx.doi.org/10.1080/01496395.2010.487721.

[37] Z. Li, R. Wnetrzak, W. Kwapinski, J.J. Leahy, Synthesis and characterization of sulfated TiO_2 nanorods and ZrO_2/TiO_2 nanocomposites for the esterification of biobased organic acid, ACS Appl. Mater. Interfaces 4 (2012) 4499–4505, http://dx.doi.org/10.1021/am300510u.

[38] R.M. Fabrao, J.F. Brito, J.L. Silva, N.R. Stradiotto, M.V.B. Zanoni, Appraisal of photoelectrocatalytic oxidation of glucose and production of high value chemicals on nanotube Ti/TiO_2 electrode, Electrochim. Acta 222 (2016) 123–132, http://dx.doi.org/10.1016/j.electacta.2016.10.164.

[39] C. Kim, S. Kim, J. Choi, J. Lee, S.J. Kang, Y.-E. Sung, J. Lee, W. Choi, J. Yoon, Blue TiO_2 nanotube array as an oxidant generating novel anode material fabricated by simple cathodic polarization, Electrochim. Acta 141 (2014) 113–119, http://dx.doi.org/10.1016/j.electacta.2014.07.062.

[40] T.T. Guaraldo, S.H. Pulcinelli, M.V.B. Zanoni, Influence of particle size on the photoactivity of Ti/TiO_2 thin film electrodes, and enhanced photoelectrocatalytic degradation of indigo carmine dye, J. Photochem. Photobiol. A Chem. 217 (2011) 259–266, http://dx.doi.org/10.1016/j.jphotochem.2010.10.019.

[41] A. Markowska-Szczupak, K. Wang, P. Rokicka, M. Endo, Z. Wei, B. Ohtani, A.W. Morawski, E. Kowalska, The effect of anatase and rutile crystallites isolated from titania P25 photocatalyst on growth of selected mould fungi, J. Photochem. Photobiol. B Biol. 151 (2015) 54–62, http://dx.doi.org/10.1016/j.jphotobiol.2015.07.002.

[42] Z. Rui, S. Wu, C. Peng, H. Ji, Comparison of TiO_2 Degussa P25 with anatase and rutile crystalline phases for methane combustion, Chem. Eng. J. 243 (2014) 254–264, http://dx.doi.org/10.1016/j.cej.2014.01.010.

[43] J. Wang, Y. Yu, S. Li, L. Guo, E. Wang, Y. Cao, Doping behavior of Zr^{4+} ions in Zr^{4+}-doped TiO_2 nanoparticles, J. Phys. Chem. C 117 (2013) 27120–27126, http://dx.doi.org/10.1021/jp407662d.

[44] G.G. Bessegato, T.T. Guaraldo, J.F. Brito, M.F. Brugnera, M.V.B. Zanoni, Achievements and trends in photoelectrocatalysis: from environmental to energy applications, Electrocatalysis 6 (2015) 415–441, http://dx.doi.org/10.1007/

s12678-015-0259-9.
[45] J.F. Brito, M.V.B. Zanoni, On the application of Ti/TiO_2/CuO n-p junction semiconductor: a case study of electrolyte, temperature and potential influence on CO_2 reduction, Chem. Eng. J. 318 (2016) 264–271, http://dx.doi.org/10.1016/j.cej.2016.08.033.
[46] J. Tauc, R. Grigorov, A. Vancu, Optical properties and electronic structure of amorphous Germanium, Phys. Status Solidi 15 (1966) 627–637, http://dx.doi.org/10.1002/pssb.19660150224.
[47] M.M. Mikhailov, A.C. Verevkin, The variation of band gap width in zirconium oxide powders on grinding, Russ. Phys. J. 47 (2004) 600–604, http://dx.doi.org/10.1023/B:RUPJ.0000047840.56967.3d.
[48] M. Bensitel, O. Saur, J. Lavalley, Acidity of zirconium oxide and sulfated ZrO_2 samples, Mater. Chem. Phys. 17 (1987) 249–258, http://dx.doi.org/10.1016/0254-0584(87)90147-7.
[49] C.M. Sánchez-Sánchez, V. Montiel, D. Tryk, A. Aldaz, A. Fujishima, Electrochemical approaches to alleviation of the problem of carbon dioxide accumulation, Pure Appl. Chem. 73 (2001) 1917–1927, http://dx.doi.org/10.1351/pac200173121917.
[50] S. Kaneco, Y. Shimizu, K. Ohta, T. Mizuno, Photocatalytic reduction of high pressure carbon dioxide using TiO_2 powders with a positive hole scavenger, J. Photochem. Photobiol. A Chem. 115 (1998) 223–226, http://dx.doi.org/10.1016/S1010-6030(98)00274-3.
[51] T. Mizuno, K. Adachi, K. Ohta, A. Saji, Effect of CO_2 pressure on photocatalytic reduction of CO_2 using TiO_2 in aqueos solutions, J. Photochem. Photobiol. A Chem. 98 (1996) 87–90, http://dx.doi.org/10.1016/1010-6030(96)04334-1.
[52] H. Zhou, Y. Zhang, Electrochemically self-doped TiO_2 nanotube arrays for supercapacitors, J. Phys. Chem. C 118 (2014) 5626–5636, http://dx.doi.org/10.1021/jp4082883.
[53] J. Peng, G. Li, H. Chen, D. Wang, X. Jin, G.Z. Chen, Cyclic voltammetry of ZrO_2 powder in the metallic cavity electrode in molten $CaCl_2$, J. Electrochem. Soc. 157 (2010) F1–F9, http://dx.doi.org/10.1149/1.3244568.
[54] J.F. Brito, A.S. Alves, A.J. Cavalheiro, M.V.B. Zanoni, Evaluation of the parameters affecting the photoelectrocatalytic reduction of CO_2 to CH_3OH at Cu/Cu_2O electrode, Int. J. Electrochem. Sci. 9 (2014) 5961–5973.
[55] G. Ghadimkhani, N.R. de Tacconi, W. Chanmanee, C. Janaky, K. Rajeshwar, Efficient solar photoelectrosynthesis of methanol from carbon dioxide using hybrid CuO-Cu_2O semiconductor nanorod arrays, Chem. Commun. 49 (2013) 1297–1299, http://dx.doi.org/10.1039/c2cc38068d.
[56] H. Peng, J. Lu, C. Wu, Z. Yang, H. Chen, W. Song, P. Li, H. Yin, Co-doped MoS_2 NPs with matched energy band and low overpotential high efficiently convert CO_2 to methanol, Appl. Surf. Sci. 353 (2015) 1003–1012, http://dx.doi.org/10.1016/j.apsusc.2015.06.178.
[57] P. Clechet, J. Martin, R. Olier, C. Vallouy, Photoelectrochemical effect of several transition metal oxides, Acad. Sci. Paris 282 (1976) 887.
[58] H. Maruska, A.K. Ghosh, Photocatalytic decomposition of water at semiconductor electrodes, Sol Energy 20 (1978) 443–448, http://dx.doi.org/10.1016/0038-092X(78)90061-0.
[59] M.R. Singh, E.L. Clark, A.T. Bell, Effects of electrolyte, catalyst, and membrane composition and operating conditions on the performance of solar-driven electrochemical reduction of carbon dioxide, Phys. Chem. Chem. Phys. 17 (2015) 18924–18936, http://dx.doi.org/10.1039/c5cp03283k.
[60] J. Condor, K. Asghari, D. Unatrakarn, Experimental results of diffusion coefficient of sulfate ions in cement type 10 and class G, Energy Procedia 4 (2011) 5267–5274, http://dx.doi.org/10.1016/j.egypro.2011.02.506.
[61] Y. Jia, Y. Xu, R. Nie, F. Chen, Z. Zhu, J. Wang, H. Jing, Artificial photosynthesis of methanol from carbon dioxide and water via a Nile red-embedded TiO_2 photocathode, J. Mater. Chem. A 5 (2017) 5495–5501, http://dx.doi.org/10.1039/c6ta10231j.
[62] S. Yoshida, Y. Kohno, A New type of photocatalysis initiated by photoexcitation of adsorbed carbon dioxide on ZrO_2, Catal. Surv. Jpn. 4 (2001) 107–114, http://dx.doi.org/10.1023/A:1011403320301.